Journal of The Electrochemical Society

The Electrochemical Society
Advancing solid state & electrochemical science & technology

OPEN ACCESS

Voltage Hysteresis Model for Silicon Electrodes for Lithium Ion Batteries, Including Multi-Step Phase Transformations, Crystallization and Amorphization

To cite this article: Yang Jiang *et al* 2020 *J. Electrochem. Soc.* **167** 130533

View the article online for updates and enhancements.

This content was downloaded from IP address 155.198.10.231 on 30/10/2020 at 11:35

Journal of The Electrochemical Society, 2020 **167** 130533

Voltage Hysteresis Model for Silicon Electrodes for Lithium Ion Batteries, Including Multi-Step Phase Transformations, Crystallization and Amorphization

Yang Jiang,[1] Gregory Offer,[1,2,*] Jun Jiang,[1] Monica Marinescu,[1,2] and Huizhi Wang[1,z]

[1]*Department of Mechanical Engineering, Imperial College London, United Kingdom*
[2]*The Faraday Institution, Harwell Science and Innovation Campus, Didcot, United Kingdom*

Silicon has been an attractive alternative to graphite as an anode material in lithium ion batteries (LIBs). The development of better silicon electrodes and optimization of their operating conditions for longer cycle life require a quantitative understanding of the lithiation/delithiation mechanisms of silicon and how they are linked to the electrode behaviors. Herein we present a zero-dimensional mechanistic model of silicon anodes in LIBs. The model, for the first time, considers the multi-step phase transformations, crystallization and amorphization of different lithium-silicon phases during cycling while being able to capture the electrode behaviors under different lithiation depths. Based on the model, a linkage between the underlying reaction processes and electrochemical performance is established. In particular, the two sloping voltage plateaus at low lithiation depth are correlated with two electrochemical phase transformations and the emergence of the single broad plateau at high lithiation depth is correlated with the amorphization of c-$Li_{15}Si_4$. The model is then used to study the effects of crystallization rate and surface energy barriers, which clarifies the role of surface energy and particle size in determining the performance behaviors of silicon. The model is a necessary tool for future design and development of high-energy-density, longer-life silicon-based LIBs.

© 2020 The Author(s). Published on behalf of The Electrochemical Society by IOP Publishing Limited. This is an open access article distributed under the terms of the Creative Commons Attribution 4.0 License (CC BY, http://creativecommons.org/licenses/by/4.0/), which permits unrestricted reuse of the work in any medium, provided the original work is properly cited. [DOI: 10.1149/1945-7111/abbbba]

Manuscript submitted June 22, 2020; revised manuscript received September 8, 2020. Published October 5, 2020.

List of symbols

c_{rate}	C-rate (h^{-1})
C_z	Molar fraction of amorphous phase z
C_{cryst}	Molar fraction of c-$Li_{15}Si_4$
$E_{(j)}$	Equilibrium potential of electrochemical reaction j (V)
$E_{(j),0}$	Standard equilibrium potential of reaction j (V)
E^*	Extra potential increase induced by surface energy barrier (V)
F	Faraday constant (C mol^{-1})
ΔG^*	Surface energy barrier of amorphization (eV)
$i_{(j)}$	Current density of reaction j (A m^{-2})
$i_{(j),0}$	Reference current density of reaction j (A m^{-2})
I	Total current density (A m^{-2})
J	Nucleation rate (mol s^{-1})
k_0	Nucleation rate constant (m s^{-1})
k_{cryst}	Crystallization rate constant (s^{-1})
$m_{t,Si}$	Total specific mass of silicon (g m^{-2})
M_{si}	Molar mass of silicon (g mol^{-1})
n_s^*	Concentration of critical nuclei (mol m^{-3})
$Q_{(j)}$	Total capacity obtained through reaction j (C m^{-2})
R	universal gas constant (J mol^{-1} K^{-1})
S	Surface area of nuclei (m^2)
T	Temperature (K)
V	Electrode potential (V)
$w_{(j)}$	Interaction coefficient between neighboring ions in a host lattice
W^*	Impingement rate on the nuclei (m^3 s^{-1})
$x_{(j)}$	Fraction of occupied sites through reaction j
x_{cryst}	Molar fraction of c-$Li_{15}Si_4$
$\Delta x_{(j)}$	Fraction of the maximum inserted lithium ions through reaction j

Greek symbols

δ	Stoichiometry of super-alloyed lithium
$\eta_{(j)}$	Overpotential of reaction j (V)

Subscripts

0	Standard state
z	Amorphous phase index: 0 for a-Si, 1 for a-Li_xSi_2, 2 for a-$Li_{15}Si_4$, 3 for a-$Li_{15+\delta}$ Si_4
(j)	Reaction index

Silicon has been an attractive alternative to graphite as an anode material in lithium ion batteries (LIBs) because of its high theoretical specific capacity, abundance in the Earth's crust and environmental benignity.[1–5] Due to its alloying nature, the reaction of lithium with silicon leads to a theoretical capacity of 3579 mA h g^{-1}-Si[1], which is 10 times higher than that of graphite. However, silicon anodes suffer large volume change (up to 300%) along with high internal stress during lithiation/delithiation cycles,[1] which further leads to fracture and pulverization and accelerates battery degradation. The development of better silicon electrodes and optimization of their operating conditions for longer cycle life require a quantitative understanding of the lithiation/delithiation mechanisms of silicon and how they are linked to the electrode behaviors.

Previous studies have shown that LIBs using silicon anodes exhibit unique electrochemical behaviors. Pure crystalline silicon electrodes were found to have two distinctive voltage profiles between the first and subsequent cycles. During the initial lithiation, a broad flat voltage plateau at ~0.1 V (vs Li/Li^+) was observed.[6,7] While in the subsequent cycles, the voltage plateau disappeared and the charge (lithiation) curves changed to be sloping-shaped.[6] The electrochemical behaviors of silicon electrodes also depend on lithiation depth.[8] The charge and discharge voltage curves were found to be round shaped without any distinct voltage plateau when the lower cut-off voltage was higher than 0.05 V. However, further alloying silicon electrodes to below ~0.05 V would lead to a single wide voltage plateau at about 0.4 V in their de-lithiation process, resulting in an asymmetric voltage hysteresis. The size of silicon particles was also found to affect the electrode behaviors. Using Si/C composited electrodes made of silicon powders, Saint et al.[9] found that electrodes with micron-sized Si (1–10 μm) exhibited flat delithiation voltage curves with a voltage plateau at ~0.4 V, while those with nanosized Si (10–100 nm) showed sloping curves even if fully lithiated to 0 V.[9] Interestingly, when the Si particle size was reduced to less than 20 nm, even the flat voltage plateau in the first lithiation process became a sloping shape.[10,11]

*Electrochemical Society Member.
[z]E-mail: huizhi.wang@imperial.ac.uk

Several efforts have been made in recent years to understand the mechanisms underlying those unique electrode behaviors. Mechanistic studies of the first lithiation of crystalline silicon were performed independently by Limthongkul et al.,[12] Chon et al.[13] and Liu et al.[14] respectively using X-ray diffraction (XRD), scanning electron microscopy (SEM) and high-resolution electron microscopy (HRTEM). These independent, complementary studies revealed that the amorphization of crystalline silicon (c-Si) proceeded layer by layer following a "peeling off" mechanism, indicating a two-phase reaction. This can explain the broad flat voltage plateau at ~0.1 V. In the subsequent cycles, the amorphous intermediate phase a-Li_xSi was found not to recrystallize to c-Si,[6] which can be the reason for the sloping shape of the voltage curves. In situ XRD measurements were carried out by Li et al.[8] under different lithiation depths. They showed that when the voltage fell to nearly 0 V, the highly lithiated amorphous Li_xSi phase crystallized rapidly into a metastable $Li_{15}Si_4$ at the end of lithiation process. Therefore, the single wide plateau at ~0.4 V in the subsequent delithiation curves can be attributable to the two-phase reaction from crystalline $Li_{15}Si_4$ (c-$Li_{15}Si_4$) to amorphous lithium-silicon phases. When the lower cut-off voltage was higher than 0.05 V, the formation of $Li_{15}Si_4$ was avoided and only a solid-solution reaction happened,[8] thereby giving a sloping voltage curve.

Despite many advances in understanding the electrochemical performance and lithiation/delithiation mechanisms of silicon electrodes, existing efforts are scattered and disjointed. There has been no systematic, quantitative research to date that has quantified the phase transformations during cycling and correlated them with the cycling behaviors of silicon electrodes. Macroscopic models have been developed for simulating the charge/discharge curves of silicon-based LIBs,[3,4,15–17] however, none of them have considered the multi-step phase transformations and crystallization/amorphization involved in the silicon electrodes. A few studies[18,19] described the lithiation-induced amorphization of crystalline silicon based on first-principles and molecular dynamics simulations, but they can hardly be used for battery cell design and optimization due to their small computational domains. Zhang[11] reviewed the lithiation/delithiation mechanisms of alloy electrode materials for LIBs and suggested that the surface (or interface) energy could play a crucial role in determining the unique behaviors of alloy materials like silicon, but they provided no quantitative evidence.

In this study, we present a zero-dimensional mechanistic model of silicon anodes in LIBs. The model, for the first time, considers the multi-step phase transformations, crystallization and amorphization of different lithium-silicon phases during cycling while being able to capture the electrode behaviors under different lithiation depths. Based on the model, a linkage between the underlying reaction processes and electrochemical performance is established. The effects of crystallization rate and surface energy barriers are analyzed, which clarifies the role of surface energy and particle size in determining the performance behaviors of silicon electrodes. The model presented can be easily extended to model full-size LIB cells with silicon additives to account for mechanical degradation associated with the heterogeneous phase changes in the silicon electrode.

Model Development

Reaction pathways and physical mechanisms.— *Reaction pathways when the lower cut-off voltage is above 0.05 V.*—When silicon is lithiated to above 0.05 V vs Li/Li^+, two distinguishable characteristic voltage peaks occur in incremental capacity analyses,[6,20,21] indicating that there exist two major structure transformations during the cycling within this voltage range. The details of the two structure transformations have been confirmed in the in situ TEM experiment by Wang et al.[22] The first step is a heterogeneous two-phase transformation from amorphous silicon (a-Si) to amorphous Li_xSi (a-Li_xSi), through which a distinct phase boundary was observed in the study of Wang et al..[6] So far, no agreement has been reached on the exact value of x, and x is generally considered less than 2.[1,8] The second step of lithiation was found to proceed without a visible interface, forming the final amorphous product a-$Li_{15}Si_4$. Based on the above evidence from the literatures, as shown in Fig. 1, a two-step reaction mechanism consisting of two reversible electrochemical steps 1 and 2 is proposed for cycling of silicon in a voltage range above 0.05 V.

Reaction pathways when the lower cut-off voltage is below 0.05 V.—When the voltage of silicon falls below 0.05 V vs Li/Li^+, another voltage plateau which is visibly short appears at the end of charge,[23] accompanied by an abrupt formation of crystalline c-$Li_{15}Si_4$.[1] The rapid appearance of a crystalline phase suggests a homogeneous crystallization from the amorphous composition of $Li_{15}Si_4$. This homogeneous crystallization process is analogous to the freezing of super-cooled water where liquid water can stay completely free of ice for a long period before being instantaneously crystallized to ice. However, the process is too fast to have been captured in any in situ studies. A homogeneous crystallization typically involves a preceding nucleation from bulk composition and a subsequent grain growth based on the existing nuclei sites.[24] Hence, it is reasonable to describe the process using a two-step mechanism, i.e., an electrochemical step f3 that forms critical nuclei of $Li_{15+\delta}Si_4$ (δ represents a very small increment of lithium) from bulk solid solution followed by a chemical step f4 that grows the nuclei to the metastable crystalline phase c-$Li_{15}Si_4$. Using the super-cooled water analogy, a "super-alloyed" phase a-$Li_{15+\delta}Si_4$ is assumed as the product of the reaction step f3,[25] which is assumed to have the local highest energy and an unstable structure. The electrochemical step f3 is driven by overpotentials which push a-$Li_{15}Si_4$ phase to overcome the surface energy barrier of forming a nucleus.[26] During the process, the original bulk phase of $Li_{15}Si_4$ is expected to grow to its critical size by accommodating more lithium ions, which explains the slight capacity increase during crystallization of $Li_{15}Si_4$.[23] The extra lithium atoms (represented by δ) are believed to act as a "catalyst" which enables the crystallization process by activating the amorphous $Li_{15}Si_4$, despite the small amount.

In contrast to the sloping voltage curve in the charge process, the discharge process exhibits a single distinct voltage plateau at ~0.4 V.[1,7] It was found by Li et al.[1] using in situ XRD that the

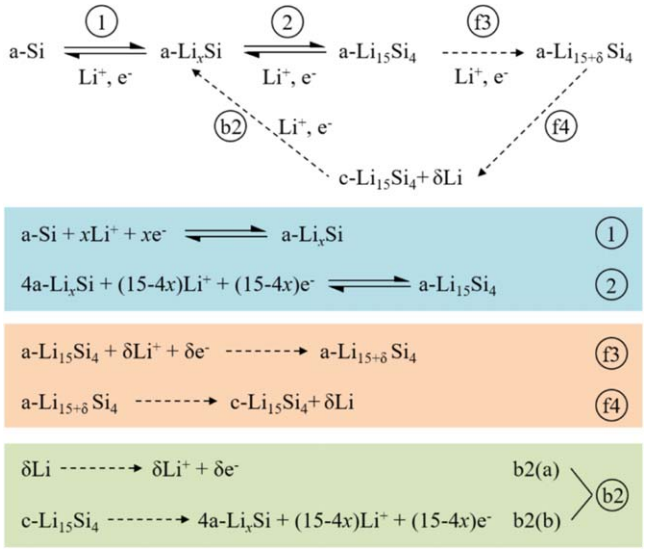


Figure 1. Reaction pathways for electrochemical lithiation and delithiation of silicon at room temperatures.

Table I. Parameter values used in base case simulations.

Parameter	Unit	Value	Comment/reference
δ		0.01	Assumed
$E_{(1),0}/E_{(2),0}$	V	0.375/0.18	Ref. 11
$E_{(f3),0}$	V	0.053	Ref. 23
E^*	V	0.15	Estimated based on the surface energy gap between amorphous and crystalline silicon reported in Refs. 29, 30
$i_{(1),0}/i_{(2),0}$	A m^{-2}	0.002/ 0.008	Assumed
$i_{(f3),0}/i_{(b2),0}$	A m^{-2}	0.008/ 0.004	Assumed
k_{cryst}	s^{-1}	0.00036	Assumed
$w_{(1)}/w_{(2)}$		1.5/1.0	Ref. 20
$w_{(f3)}/w_{(b2)}$		1.0/1.0	Ref. 20
x		1.6	Fitted for Ref. 8

crystalline $Li_{15}Si_4$ disappeared linearly with time under a galvanostatic condition. These experimental findings indicate a two-phase heterogeneous amorphization process of c-$Li_{15}Si_4$. The linear decrease of crystalline phase under constant current conditions implies that this amorphization process is rate determining. Previous studies[1] suggested that the product of the amorphization process could be a-Li_xSi. Ignoring the reaction of the extra lithium atoms b2 (a) ($\delta \ll 15$), here we assume that the amorphization of c-$Li_{15}Si_4$ follows the reaction step b2(b) to end up with the same product of the reaction step 1, in view of the metastable structure of the intermediate product.

Pathway diagram.—The proposed pathways of electrochemical lithiation/delithiation of silicon at room temperatures are summarised in Fig. 1. The lithiation/delithiation process follows a two-step mechanism consisting of two reversible electrochemical steps 1 and 2 when the electrode potential is maintained above 0.05 V, and will undergo homogeneous crystallization steps f3 and f4 for lithiation and heterogeneous amorphization b2 for delithiation when the electrode potential goes below 0.05 V.

Electrochemical reactions.— *Thermodynamics.*—The equilibrium potentials of electrochemical reactions 1, f3 and b2 are calculated as[27,28]:

$$E_{(j)} = E_{(j),0} + \frac{w_{(j)}}{f} \ln\left(\frac{\Delta x_{(j)} - x_{(j)}}{x_{(j)}}\right) \quad [1]$$

$$f = F/RT \quad [2]$$

where $E_{(j)}$ and $E_{(j),0}$ are respectively the equilibrium potential (V) and standard equilibrium potential (V) of reaction j (j = 1, 2, f3, b2), F is the Faraday constant ($F = 96485$ s A mol^{-1}), R is the universal gas constant ($R = 8.314$ J mol^{-1} K^{-1}), T is the temperature (K) and $w_{(j)}$ is an adjustable parameter describing the interactions between transferred electric charge and its surrounding in reaction j. It is noted that Eq. 1 is a general description of equilibrium potential, which accounts for the short-range interactions between neighboring ions (via $w_{(j)}$) and has been widely used in the literatures. An detailed interpretation of the parameter $w_{(j)}$ can be found in the literatures.[27,28] The term ($\Delta x_{(j)}$-$x_{(j)}$) represents the remaining vacant sites for lithium through reaction j, where $\Delta x_{(j)}$ is the fraction of total host sites for lithium ions through reaction j and $x_{(j)}$ is the fraction of the already occupied sites in that reaction. For each electrochemical reaction, the fraction of total host sites for lithium ions, $\Delta x_{(j)}$, is calculated as the ratio of the maximum capacity through that reaction ($Q_{(j)}$) to the total capacity when silicon is fully lithiated (Q_{tot}) and can be further expressed in terms of the compositions of reactants and products

$$\Delta x_{(1)} = \frac{Q_{(1)}}{Q_{tot}} = \frac{x}{3.75 + \delta/4} \quad [3]$$

$$\Delta x_{(2)} = \Delta x_{(b2)} = \frac{Q_{(2)}}{Q_{tot}} = \frac{3.75 - x}{3.75 + \delta/4} \quad [4]$$

$$\Delta x_{(f3)} = \frac{Q_{(f3)}}{Q_{tot}} = \frac{\delta/4}{3.75 + \delta/4} \quad [5]$$

The values x, 3.75 and (3.75 + δ/4) on the right hand side of the above equations are the average lithium/silicon ratios of host structures [a-Li_xSi], [a-$Li_{15}Si_4$] and [a-$Li_{15+\delta}Si_4$].

The total capacity, Q_{tot}, is related to the specific mass of silicon, $m_{t,Si}$, by

$$Q_{tot} = (3.75 + \delta/4)\frac{m_{t,Si}F}{M_{Si}} \quad [6]$$

where M_{si} is the molar mass of silicon ($M_{si} = 28$ g mol^{-1}). It is noted that the sum of $\Delta x_{(j)}$ (j = 1, 2, f3) should be equal to 1.

Electrochemical amorphization.—Reaction b2, the heterogeneous amorphization of c-$Li_{15}Si_4$, occurs only on the crystalline

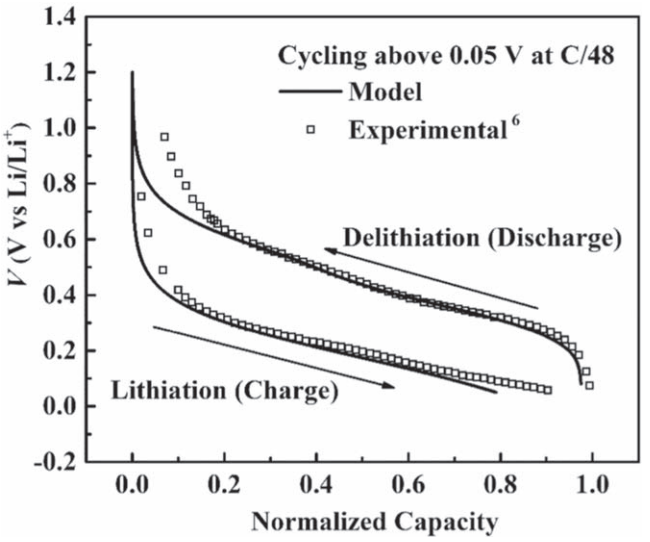


Figure 2. Comparison of model predictions with the experimental data for an amorphous silicon electrode operating at voltages above 0.05 V.

surface where the atoms have higher free energy than the interior ones, thereby following a "peeling off" pattern. Compared to the conversion of a-$Li_{15}Si_4$ to a-Li_xSi in reaction 2, the amorphization of c-$Li_{15}Si_4$ to a-Li_xSi needs to overcome an extra energy barrier ΔG^*(eV)

$$\Delta G_{(2b),0} = \Delta G_{(2),0} + \Delta G^* \quad [7]$$

where $\Delta G_{(2b),0}$ and $\Delta G_{(2),0}$ respectively denote the standard Gibbs energy changes of reactions b2 and 2. The change in the Gibbs free energy leads to a higher equilibrium potential of reaction b2 than that of reaction 2

$$E_{(b2),0} = \frac{\Delta G_{(2b),0}}{(3.75 - x)e} = \frac{\Delta G_{(2),0} + \Delta G^*}{(3.75 - x)e} = E_{(2),0} + E^* \quad [8]$$

where e is the elementary charge ($e = 1.6 \times 10^{-19}$ A s), and E^* is an extra voltage increase induced by the surface energy barrier ΔG^* (V). In Eq. 8, the Gibbs free energy changes are all positive since the delithiation process is nonspontaneous.

Charge transfer kinetics.—The reaction rate for each electrochemical steps 1, 2, f3 and b2 is assumed to follow a simplified Butler-Volmer equation,

$$i_{(j)} = -2i_{(j),0} \sinh\left(\frac{f\eta_{(j)}}{2}\right) \quad [9]$$

where $i_{(j)}$ is the current density (A m^{-2}) for reaction j and $i_{(j),0}$ is the reference current density (A m^{-2}) of reaction j. $i_{(j)}$ is defined to be positive for charge and negative for discharge. $\eta_{(j)}$ is the overpotential (V) of reaction j, and expressed as

$$\eta_{(j)} = V - E_{(j)} \quad [10]$$

where V is the electrode potential (V).

The total current density of the silicon electrode, I, is the sum of the partial current densities

$$I = \sum_j i_{(j)} \quad [11]$$

Crystallization kinetics.—As discussed before, the crystallization of a-$Li_{15}Si_4$ involves an electrochemical nucleation step (f3) followed by a crystal growth step (f4). The kinetics of the reaction f4 can be described using the classical nucleation theory[24]

$$J = W^* n_s^* \quad [12]$$

where J is nucleation rate (mol s^{-1}) and n_s^* is the near equilibrium concentration of critical nuclei (mol m^{-3}). W^* is the rate of the condensable species upon these nuclei through impingement (m^3 s^{-1}), which is proportional to the surface area of the nuclei S[24]

$$W^* = k_0 S \quad [13]$$

where k_0 is the rate constant of crystallization.

Based on the classical nucleation theory, here we develop a heuristic kinetic expression for reaction step f4

$$\frac{dx_{cryst}}{dt} = k_{cryst} x_{cryst}\left(\frac{x_{(f3)}}{\Delta x_{(f3)}} - x_{cryst}\right) \quad [14]$$

where $(\frac{x_{(f3)}}{\Delta x_{(f3)}} - x_{cryst})$, analogous to n^*, represents the remaining fraction of critical nuclei which should minus the already crystallized portion x_{cryst}; x_{cryst}, analogous to S, represents the surface for crystal growth. The crystallization growth rate can also be lumped to

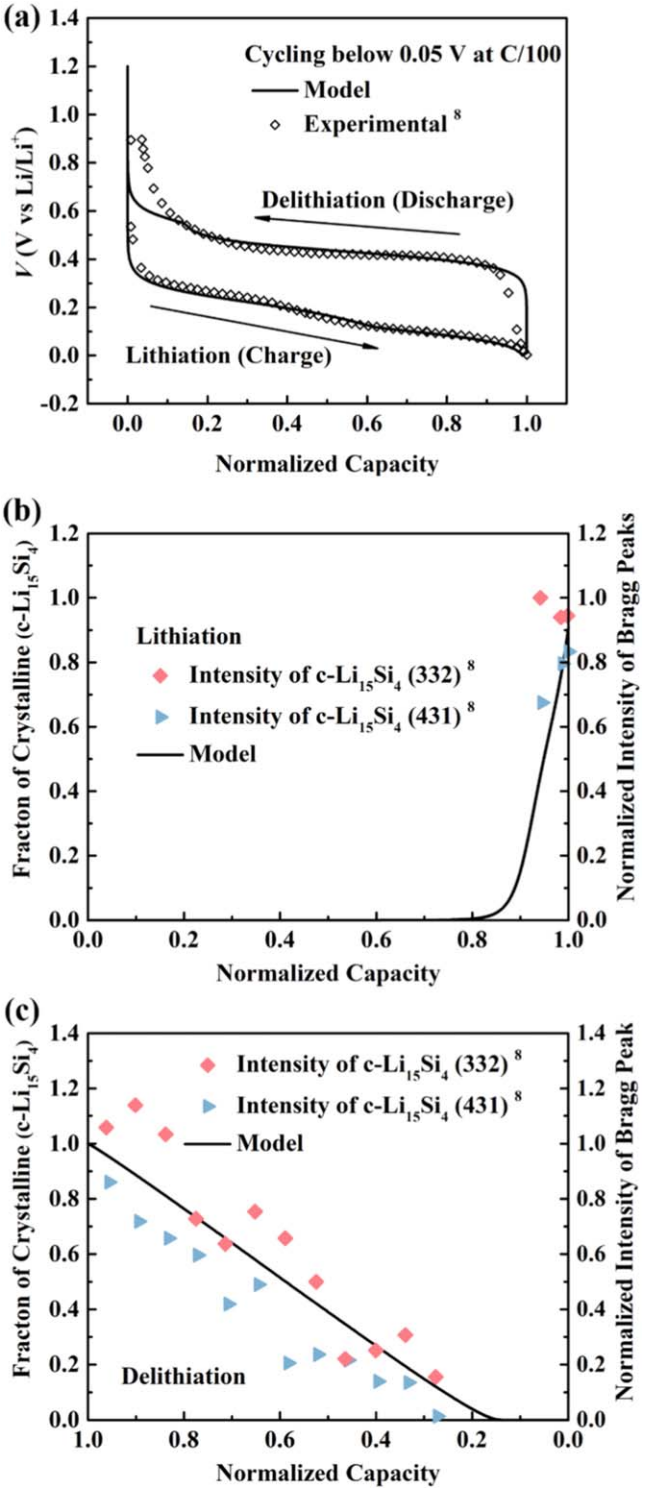


Figure 3. Comparison of model predictions with the experimental data below 0.05 V: (a) charge/discharge curves and concentration variation of c-$Li_{15}Si_4$ during (b) charge and (c) discharge.

$k^*_{cryst} = k_{cryst}\left(\frac{x_{(f3)}}{\Delta x_{(f3)}} - x_{cryst}\right)$, which implies that the real growth rate is restricted by the depletion of the parent nuclei [a-$Li_{15+\delta}Si_4$].

Time evolution of species.—By ignoring spatial heterogeneity within silicon electrode, the rate of change in the molar fraction of the inserted lithium for each electrochemical reaction is given by

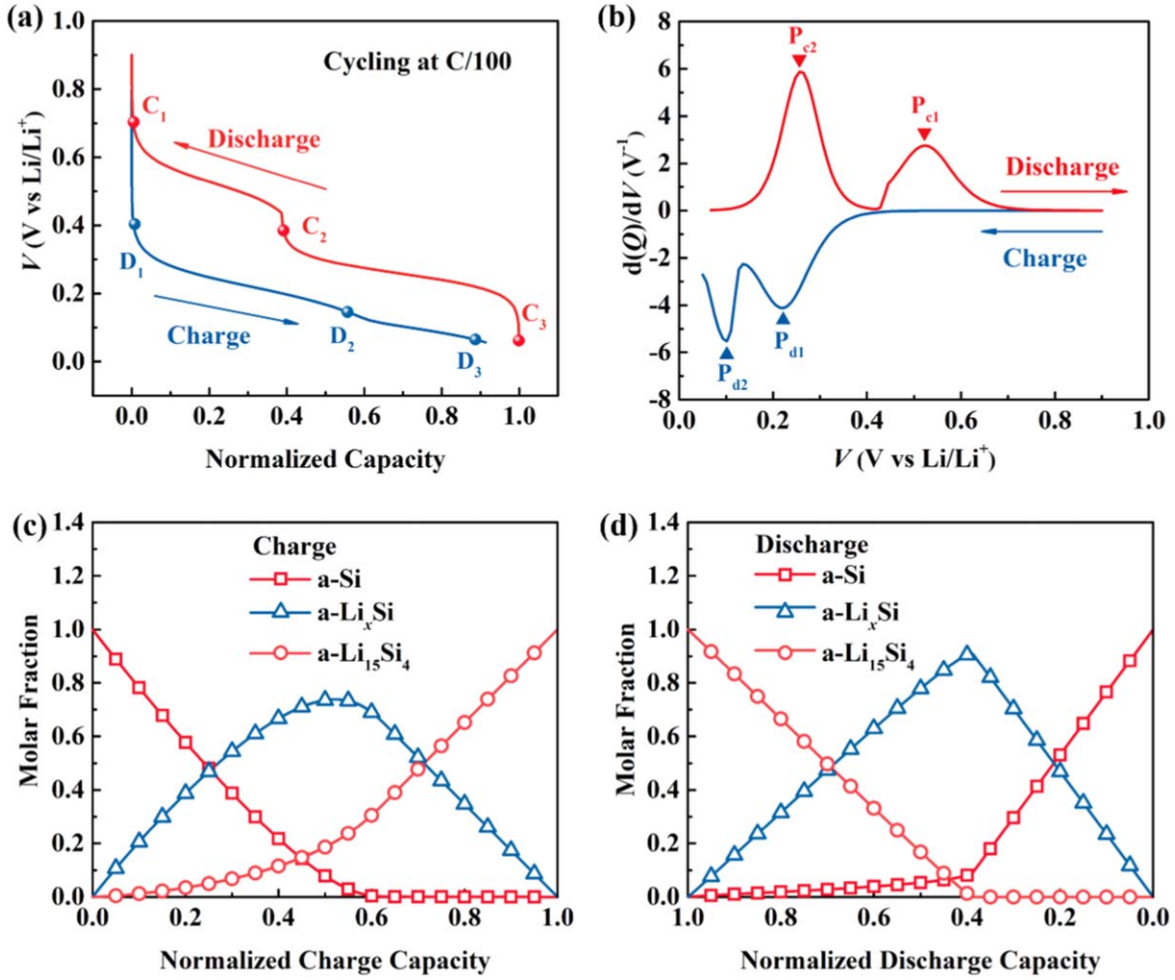


Figure 4. Electrochemical behaviors and phase transformations of silicon in the absence of crystallization during discharge and charge: (a) voltage curves; (b) differential voltage curves; and composition variations during (c) charge and (d) discharge.

$$\frac{dx_{(j)}}{dt} = \frac{i_{(j)}}{Q_{tot}} \quad [15]$$

In the absence of crystallization, the normalized concentrations of a-Si, a-Li_xSi and a-$Li_{15}Si_4$ are expressed in the fraction of occupied sites

$$C_0 = 1 - \frac{x_{(1)}}{\Delta x_{(1)}} \text{ for a-Si} \quad [16]$$

$$C_1 = \frac{x_{(1)}}{\Delta x_{(1)}} - \frac{x_{(2)}}{\Delta x_{(2)}} \text{ for a-Li}_x\text{Si} \quad [17]$$

$$C_2 = \frac{x_{(2)}}{\Delta x_{(2)}} \text{ for a-Li}_{15}\text{Si}_{14} \quad [18]$$

In the presence of crystallization, the normalized concentration of a-$Li_{15}Si_4$ becomes

$$C_2 = \frac{x_{(2)}}{\Delta x_{(2)}} - \frac{x_{(f3)}}{\Delta x_{(f3)}} \quad [19]$$

and the normalized concentrations of the critical nuclei and crystalline phase are calculated by

$$C_3 = \frac{x_{(f3)}}{\Delta x_{(f3)}} - x_{cryst} \text{ for critical nuclei} \quad [20]$$

$$C_{cryst} = x_{cryst} \text{ for crystalline phase} \quad [21]$$

Computational implementation and initial conditions.—The model consists of differential equations Eqs. 1, 9–11, 14 and 15 for (4j + 2) unknowns: $x_{(j)}$, x_{cryst}, $i_{(j)}$, V, $\eta_{(j)}$ and $E_{(j)}$. The fractions C_z and C_{cryst} are further determined using Eqs. 16–21 with the values of $x_{(j)}$ and x_{cryst} solved from the differential equation system. The equation system was solved by the Runge–Kutta method using MATLAB ode23t. The initial conditions for all variables were calculated self consistently from chosen values of V and x_{cryst} for charge and V for discharge. The partial current densities were initialized as $i_{(1)} = I$, $i_{(j)} = 0$ (j = 2, f3) for charge and $i_{(2)}/i_{(b2)} = I$, $i_{(1)} = 0$ for discharge.

The values of model parameters used for base case simulations are summarized in Table I. The lithium/silicon ratio in a-Li_xSi is fitted to be 1.6 from the experimental data[8] used in this study. The potential increase in amorphization E^* is set to be 0.15 V, corresponding to a surface energy gap of 0.3225 eV/atom. This has the same order of magnitude as the energy gap between amorphous and crystalline bulk silicon.[29,30] The values of reference current densities

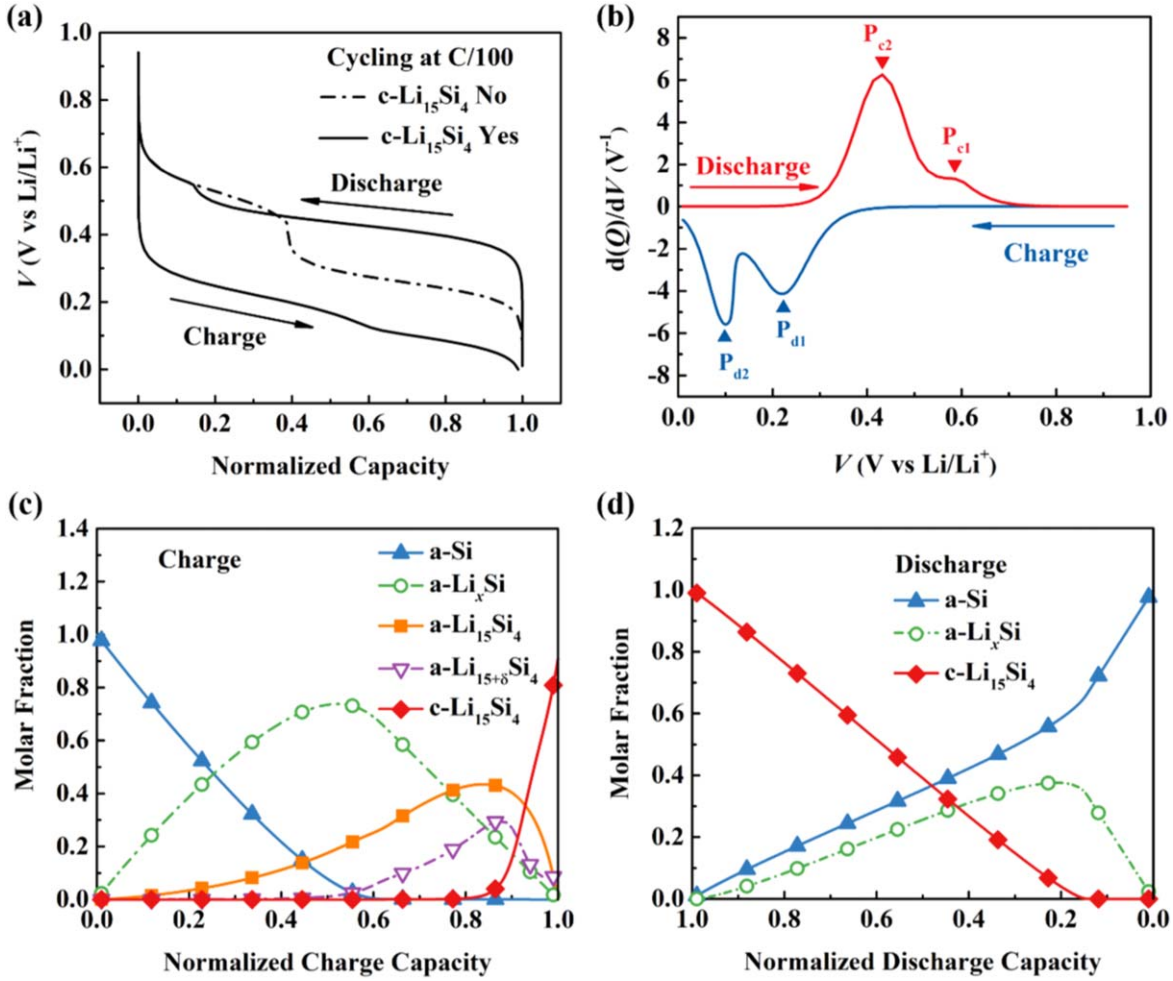


Figure 5. Electrochemical behaviors and phase transformations of silicon in the presence of crystallization during discharge and charge: (a) voltage curves; (b) differential voltage curves; and composition variations during (c) charge and (d) discharge.

varies dramatically in the literatures,[17,31–33] ranging from 1 to 10^9 A m^{-2}. Here we assume the values of reference current density to be 0.002, 0.008, 0.008 and 0.004 A m^{-2} respectively for reactions 1, f3 and b2 due to the lack of precise experimental data. Although internal stress can also be attributed to the voltage gap between lithiation and de-lithiation curves of silicon electrodes,[5,31] we only consider the kinetic contribution to the hysteresis in this study. The adjustable parameter $w_{(j)}$ were reported in a range of 0.7–6.0,[20] and we take the values of 1.5 and 1.0 for different reaction steps. All simulations are performed at 298 K.

Results and Discussion

Model-experiment comparisons.—Figure 2 compares the model results with the experimental data reported in the literature.[6] The simulated charge-discharge curves agree well with the measured ones. As can be seen in the figure, the model successfully reproduces the sloping voltage curves of both charge and discharge processes when the amorphous silicon electrode is cycled above 0.05 V (vs Li/Li$^+$). The voltage curves of discharge and charge processes appear to be approximately parallel to each other with a huge voltage hysteresis in between which is caused by sluggish kinetics (small i_0). The model is further validated against the experimental data for deep lithiation of silicon.[8] It can be seen in Fig. 3a that the model results are consistent with experimental results by showing the same asymmetric feature, where the charge curve exhibits a sloping shape and the discharge curve has a single voltage plateau. For both scenarios of >0.05 V and <0.05 V, it is noted that the biggest difference between our model and experimental results occurs at the end of discharge (EOD) and the end of charge (EOC). This can be caused by asymmetric internal stress, which makes a larger voltage hysteresis at the EOD than that at the EOC.[5] Hence, the neglect of the stress effect in this study may lead to an underestimation of voltage hysteresis at the EOD and an overestimation of voltage hysteresis at the EOC.

The predicted composition change during deep cycling is compared with the XRD results in Figs. 3b and 3c. As shown in Fig. 3b, a sudden formation of c-$Li_{15}Si_4$ at a charge voltage of 0.05 V is shown in both the model predictions and experimental measurements. Figure 3c shows that the linear decrease of c-$Li_{15}Si_4$ observed by in situ XRD is also well captured by our model.

It is worth mentioning that the asymmetric voltage hysteresis as well as phase changes of silicon electrodes have never been well described by previous models which have taken into account various types of overpotential (i.e., charge-transfer, diffusion and ohmic overpotentials) and internal mechanical stresses.[5,34]

Charge/discharge behavior.—The model is used to study the charge/discharge behaviors of silicon in details. Figures 4a and 4b respectively show the charge/discharge curves and the corresponding differential voltage spectroscopy when silicon is lithiated above 0.05 V. The sigmoidal shaped voltage curve with two sloping plateaus in Fig. 4a as well as its associated characteristic peaks in Fig. 4b have been widely reported in experimental studies on silicon electrodes.[35,36] This sigmoidal shape is a typical feature of electrochemical phase changes, and the voltage tends to hold during each

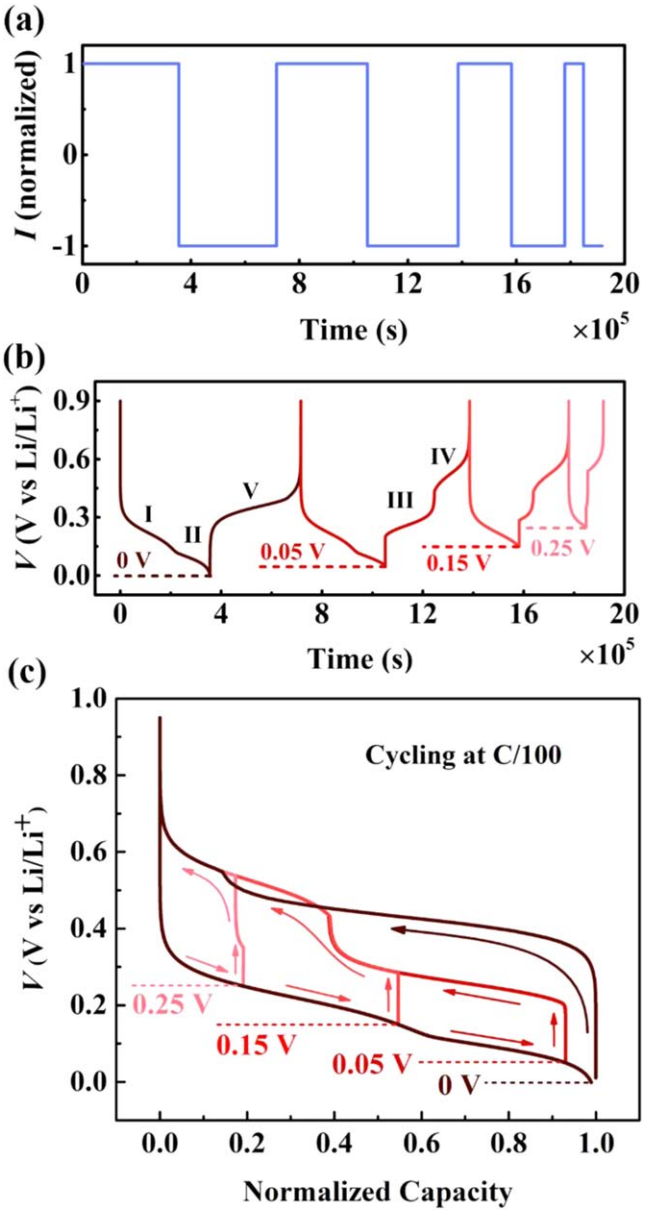


Figure 6. Electrochemical behaviors of silicon cycled between different voltage limits: (a) current density vs time; (b) voltage vs time; (c) voltage loops.

phase transformation process, thus exhibiting a voltage plateau during charge/discharge. In Fig. 4a, both the charge and discharge curves have two voltage plateaus which imply two transformation reactions, i.e., reactions 1 and 2. The voltage characteristic peaks in Fig. 4b suggest that the two discharge reactions respectively happen at 0.25 and 0.52 V vs Li/Li^+, while the two charge reactions occur at 0.11 and 0.22 V vs Li/Li^+. The variations of different silicon phases during cycling are further examined in Figs. 4c and 4d. When silicon is charged from D_1 to D_2 (Fig. 4a), it is seen in Fig. 4c that a-Si declines almost linearly and a-Li_xSi increases at the same time, and reaction 1 dominates over reaction 2. It is also found that a-$Li_{15}Si_4$ grows slower than a-Li_xSi in the D_1-D_2 regime, confirming that reaction 2 is a slower step in this regime. When silicon is further charged from D_2 to D_3, a-Li_xSi stops growing and transforms to a-$Li_{15}Si_4$ via reaction 2. These two electrochemical reactions proceed in the reverse direction during discharge. It is shown in Fig. 4d that a-$Li_{15}Si_4$ will firstly transform to a-Li_xSi, followed by the phase transformation from a-Li_xSi to a-Si.

The charge/discharge behaviors and the corresponding phase transformations for cycling silicon below 0.05 V are studied in Fig. 5. In contrast to Fig. 4a, the lower voltage plateau is elevated and even merges with the higher plateau during the discharge process in Fig. 5a, which displays a wide voltage plateau at ~0.4 V. This phenomenon is confirmed in Fig. 5b, where P_{c2} moves to a higher voltage level and P_{c1} becomes unnoticeable. Figures 5a and 5b confirm that the electrochemical behaviors of silicon electrodes are path-dependent: (a) When the voltage remains higher than 0.05 V, silicon only follows the lithiation steps 1 and 2, leading to two sloping plateaus during both charge and discharge; (b) When the voltage falls below 0.05 V, silicon will undergo an additional crystallization process, thereby showing a distinct flat voltage plateau during de-lithiation. Figure 5c shows variation of different silicon phases during charge. It is found that the initial two electrochemical steps are similar to those in Fig. 4c, where a-Si is firstly lithiated to form a-Li_xSi before transforming to a-$Li_{15}Si_4$. The nucleation step f3 starts at a normalized capacity of ~0.5, slowing down the formation of a-$Li_{15}Si_4$ in the second half of the capacity range. At the same time, the critical nuclei a-$Li_{15+\delta}Si_4$ starts to grow until it reaches to a fraction of 0.3, and then the fraction of c-$Li_{15}Si_4$ starts to increase exponentially. For the reverse process, Fig. 5d shows that c-$Li_{15}Si_4$ is firstly amorphized to a-Li_xSi which is further delithiated to form a-Si. Compared to the case in Fig. 4d, the fraction of a-Si in the reverse process grows at the beginning, indicating that the reaction rate of step 1 is comparable to that of step b2 through the discharge process. In addition, the maximum fraction of a-Li_xSi is found to be less than 0.4, which is less than half of that in Fig. 4d. Surprisingly, the depletion of $Li_{15}Si_4$ delays from the normalized capacity of 0.4 to 0.15. During the whole discharge process, the silicon electrode is composed of a mixture of a-Li_xSi and a-Si during amorphization, which implies that there may be no pure intermediate component.

Figure 6 shows the electrochemical behaviors of silicon during micro-cycling operation between different voltage limits. The transition from the lower lithiation voltage branch to the upper lithiation voltage branch for silicon electrodes was well identified and explained by Baker et al.[37] in a slow voltage scan. In Fig. 6, the silicon electrode is cycled at C/100, and the current is reversed immediately after the lower voltage limit is reached. In Fig. 6b, during the first cycle when the voltage falls to 0 V, the silicon electrode undergoes two phase transformation stages I and II, respectively corresponding to the reaction steps 1 and 2. After the current is reversed, the voltage curve presents a distinct plateau V which suggests the amorphization process b4. In the subsequent cycles, at lower voltage limits of 0.05 V, 0.15 V and 0.25 V, the lower voltage branch (lithiation branch) follows the same trace as that in the first cycle, while the higher voltage branch turns to be sigmoidal. The last three cycles do not involve crystallization thus exhibit two sloping plateaus in de-lithiation voltage curves as shown in Figs. 6b and 6c, where the stages III and IV respectively correspond to the reaction steps 1 and 2. It is worth mentioning that when the lower voltage limit increases, the first voltage plateau III in the higher voltage trace becomes shorter and can even vanish. This is because the reaction step 2 dominates at lower voltages, and the voltage plateau of the step 2 becomes less observable as the lower voltage limit increases. It is noted that in Fig. 6c the voltage increases abruptly at the step change of the current. This implies that the silicon electrode has not yet reached equilibrium when the voltage limit is reached, the voltage increase is due to the kinetic loss.

Effect of crystallization rate.—Figures 7a and 7b respectively show the effect of crystallization rate constant k_{cryst} on the growth of c-$Li_{15}Si_4$ and a-$Li_{15+\delta}Si_4$. It is seen in Fig. 7a that the slower the crystallization happens, the more abruptly the crystalline phase will appear. If k_{cryst} is very small ($<0.0002\ s^{-1}$), as shown in Fig. 7b, there will be excessive nuclei due to the slow f4, which lead to an exponential growth in silicon crystalline following the relationship

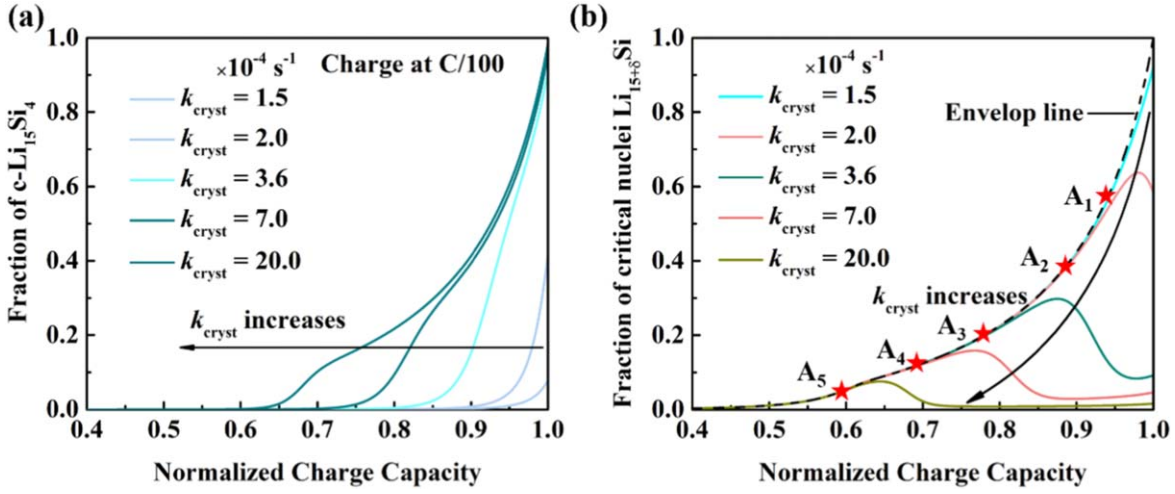


Figure 7. The effect of crystallization rate constant on the growth of (a) crystalline phase and (b) critical nuclei during charge.

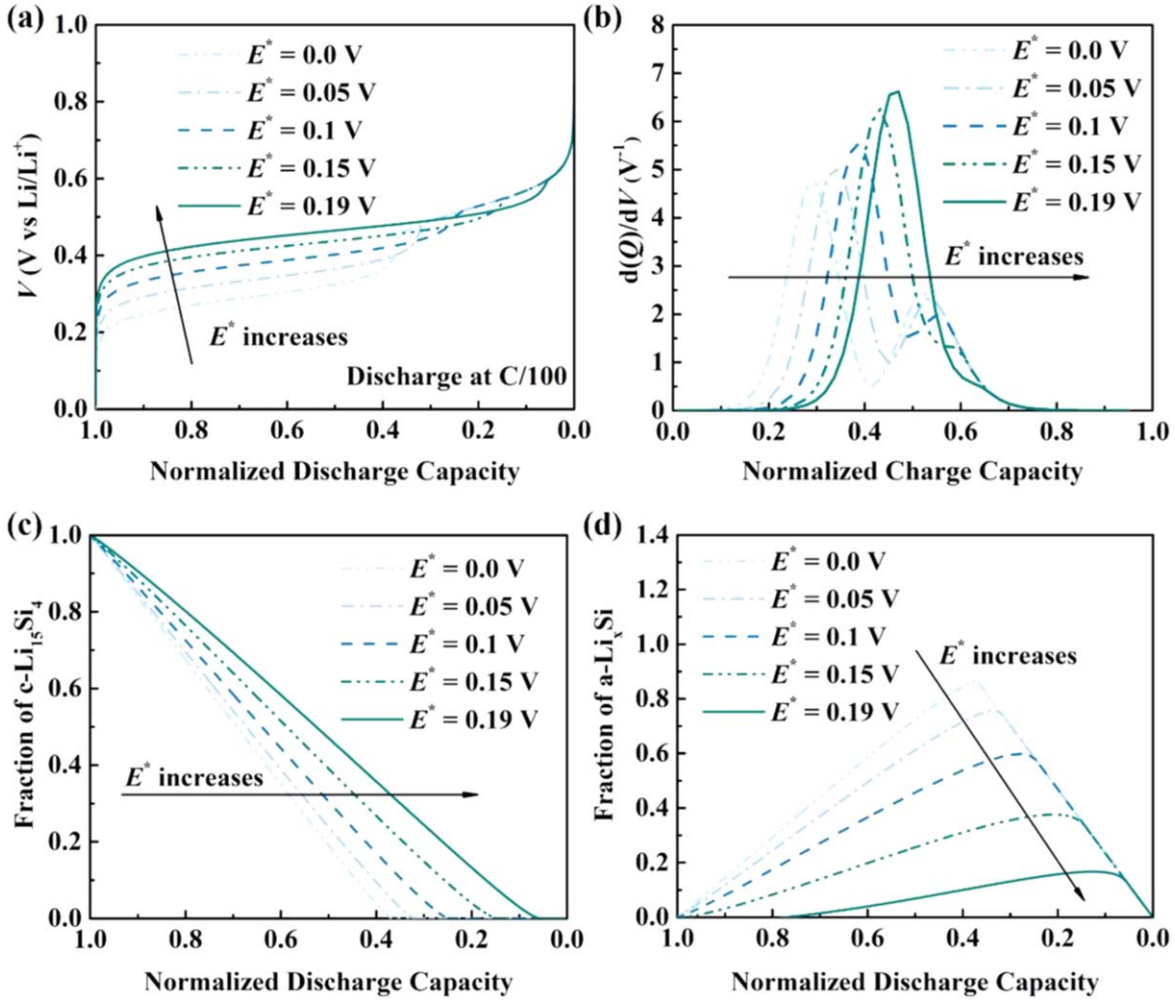


Figure 8. (a) Voltage curves, (b) differential voltage curves, and molar fraction variation of (c) c-$Li_{15}Si_4$, and (d) a-Li_xSi at different values of surface energy barrier during discharge.

$$\frac{dx_{\text{cryst}}}{dt} = k_{\text{cryst}} x_{\text{cryst}} \qquad [22]$$

As k_{cryst} increases to $0.00036\ s^{-1}$, the reaction rate of step f4 becomes comparable to that of step f3. The growth curve presents a characteristic s-shaped, or sigmoidal profile where the transformation rates are low at the beginning and the end of the process, but fast in between. This s-shaped growth curve is a typical characteristic of homogeneous crystallization.[38] If k_{cryst} is larger than $0.0007\ s^{-1}$, c-$Li_{15}Si_4$ grows fast initially until most nuclei are consumed. In this case, the crystallization rate is limited by the nucleation step f3. The

envelop line plotted in Fig. 7b is determined by $x_{(3)}/\Delta x_{(3)}$, which is equal to the total fraction of a-$Li_{15+\delta}Si_4$ and c-$Li_{15}Si_4$. The intersection points A_1-A_6 in Fig. 7b correspond to the starting points of the appearance of c-$Li_{15}Si_4$ in Fig. 7a, which tend to start earlier with increasing k_{cryst}.

Amorphization with different surface energy barriers.—The effects of surface energy barriers are studied in Fig. 8. As shown in Fig. 8a, with increasing E^*, the voltage curve during the discharge process changes from a sloping shape to a flat shape. As E^* is proportional to the extra surface energy barrier to overcome for amorphization, a larger E^* means higher surface energy barrier. When the particle size is smaller, more free surfaces of silicon phases are exposed and the silicon phases are more active on average. This elevated activity means less surface energy barrier per atom to be overcome, corresponding to a smaller E^*. Hence, a sloping voltage curve is expected during the discharge process even if the silicon particle is crystallized. This well explains the effect of particle size, which is consistent with the experimental observations in the literatures.

Figure 8b indicates that a higher surface energy barrier will shift the voltage peak to a higher level and increase its width. Furthermore, when E^* is large enough, the higher voltage peak will vanish. Hence, only one visible voltage characteristic peak can be detected in the differential analysis even though there are two phase transformation reactions. This may lead to a failure to detect the phase transformation step b2. To unveil the underlying reactions, it is necessary to use other more reliable experimental techniques to complement the results from differential analyses.

Figure 8c shows that the decrease of crystalline phase is decelerated with increasing E^* because of the slowing down in amorphization. Correspondingly, as shown in Fig. 8d, the growth of a-Li_xSi during amorphization also slows down, and the amorphization process can thus last for a longer time.

Conclusions

A zero-dimensional mechanistic voltage model is developed for silicon anodes in LIBs. The model is able to capture key electrochemical phenomena during cycling of silicon electrodes for the first time, including the sloping voltage curve with voltage hysteresis at small lithiation depths and the shift to a single distinct voltage plateau on discharge from the initial sloping curve upon deep lithiation. Comparisons show a good agreement between the model and experimental results. The processes of phase transformations, crystallization and amorphization underlying the electrode behaviors are resolved in the model. The model correlates the electrochemical behaviors of silicon with the underlying reaction processes in a quantitative manner. We show that the voltage hysteresis is path-dependent and the asymmetric hysteresis originates from asymmetric reaction pathways. The model is then used to study the effects of crystallization rate and surface energy barriers. The crystallization rate constant k_{cryst} can affect the shape of the crystalline growth curve, and a lower k_{cryst} will delay the appearance of the crystalline phase. The extra potential increase E^* induced by surface energy barriers between crystalline and amorphous phases is shown to be the underlying cause of the elevated voltage plateau for silicon electrodes. Even though there are two electrochemical reactions, the differential analysis can only detect one visible voltage peak when E^* is large enough. The surface energy barrier also explains qualitatively why smaller silicon particles present a sloping voltage curve even charged to 0 V. The model is a necessary tool for future design and development of high-energy-density, longer-life silicon-based LIBs.

Acknowledgments

This work was supported by UK Engineering and Physical Sciences Research Council (EPSRC) via grant EP/S000933/1, the Innovate UK WIZer project (TS/S005811/1) and the Faraday Institution Multiscale Modeling project (EP/S003053/1, FIRG003).

ORCID

Monica Marinescu https://orcid.org/0000-0003-1641-3371
Huizhi Wang https://orcid.org/0000-0003-2287-0544

References

1. M. T. McDowell, S. W. Lee, W. D. Nix, and Y. Cui, *Adv. Mater.*, **25**, 4966 (2013).
2. M. Pharr, K. Zhao, X. Wang, Z. Suo, and J. J. Vlassak, *Nano Lett.*, **12**, 5039 (2012).
3. H. Yang et al., *J. Mech. Phys. Solids*, **70**, 349 (2014).
4. M. Wang and X. Xiao, *J. Power Sources*, **326**, 365 (2016).
5. B. Lu et al., *Phys. Chem. Chem. Phys.*, **18**, 4721 (2016).
6. T. D. Hatchard and J. R. Dahn, *J. Electrochem. Soc.*, **151**, A838 (2004).
7. M. N. Obrovac and L. Christensen, *Electrochem. Solid-State Lett.*, **7**, A93 (2004).
8. J. Li and J. R. Dahn, *J. Electrochem. Soc.*, **154**, A156 (2007).
9. J. Saint et al., *Adv. Funct. Mater.*, **17**, 1765 (2007).
10. J. Graetz, C. C. Ahn, R. Yazami, and B. Fultz, *Electrochem. Solid-State Lett.*, **6**, A194 (2003).
11. W. J. Zhang, *J. Power Sources*, **196**, 877 (2011).
12. P. Limthongkul, Y.-I. Jang, N. J. Dudney, and Y.-M. Chiang, *Acta Mater.*, **51**, 1103 (2003).
13. M. J. Chon, V. A. Sethuraman, A. McCormick, V. Srinivasan, and P. R. Guduru, *Phys. Rev. Lett.*, **107**, 45503 (2011).
14. X. H. Liu et al., *Nat. Nanotechnol.*, **7**, 749 (2012).
15. A. F. Bower, P. R. Guduru, and V. A. Sethuraman, *J. Mech. Phys. Solids*, **59**, 804 (2011).
16. R. Chandrasekaran, A. Magasinski, G. Yushin, and T. F. Fuller, *J. Electrochem. Soc.*, **157**, A1139 (2010).
17. M. Wang, X. Xiao, and X. Huang, *J. Power Sources*, **348**, 66 (2017).
18. S. C. Jung and Y.-K. Han, *Electrochim. Acta*, **62**, 73 (2012).
19. V. L. Chevrier and J. R. Dahn, *J. Electrochem. Soc.*, **156**, A454 (2009).
20. M. Verbrugge, D. Baker, and X. Xiao, *J. Electrochem. Soc.*, **163**, A262 (2016).
21. J.-B. Kim, S.-H. Lim, and S.-M. Lee, *J. Electrochem. Soc.*, **153**, A455 (2006).
22. J. W. Wang et al., *Nano Lett.*, **13**, 709 (2013).
23. M. Klett, J. A. Gilbert, K. Z. Pupek, S. E. Trask, and D. P. Abraham, *J. Electrochem. Soc.*, **164**, A6095 (2017).
24. C. E. Nicholson, *Crystallisation in emulsion and microemulsion systems*, Durham University (2006), http://etheses.dur.ac.uk/1298/.
25. C. A. Angell, *Annu. Rev. Phys. Chem.*, **34**, 593 (1983).
26. Q. Meng, Y. Rong, and T. Y. Hsu, *Phys. Rev. B*, **65**, 174118 (2002).
27. M. Verbrugge, D. Baker, B. Koch, X. Xiao, and W. Gu, *J. Electrochem. Soc.*, **164**, E3243 (2017).
28. C. R. Birkl, E. McTurk, M. R. Roberts, P. G. Bruce, and D. A. Howey, *J. Electrochem. Soc.*, **162**, A2271 (2015).
29. E. P. Donovan, F. Spaepen, D. Turnbull, J. M. Poate, and D. C. Jacobson, *J. Appl. Phys.*, **57**, 1795 (1985).
30. N. Bernstein, M. J. Aziz, and E. Kaxiras, *Phys. Rev. B*, **58**, 4579 (1998).
31. V. A. Sethuraman, V. Srinivasan, and J. Newman, *J. Electrochem. Soc.*, **160**, A394 (2013).
32. T. Swamy and Y.-M. Chiang, *J. Electrochem. Soc.*, **162**, A7129 (2015).
33. J. Li, X. Xiao, F. Yang, M. W. Verbrugge, and Y.-T. Cheng, *J. Phys. Chem. C*, **116**, 1472 (2012).
34. J. H. Ryu, J. W. Kim, Y. E. Sung, and S. M. Oh, *Electrochem. Solid-State Lett.*, **7**, A306 (2004).
35. J. B. Kim, H. Y. Lee, K. S. Lee, S. H. Lim, and S. M. Lee, *Electrochem. Commun.*, **5**, 544 (2003).
36. M. N. Obrovac and L. J. Krause, *J. Electrochem. Soc.*, **154**, A103 (2007).
37. D. R. Baker, M. W. Verbrugge, and X. Xiao, *J. Appl. Phys.*, **122** (2017).
38. M. Avrami, *J. Chem. Phys.*, **7**, 1103 (1939).